2012

A Lumped Thermal Parameter Model for Scroll Compressors Including the Solution of the Temperature Distribution along the Scroll Wraps

Marco C. Diniz
deschamps@polo.ufsc.br

Evandro L. L. Pereira

Cesar J. Deschamps

A Lumped Thermal Parameter Model for Scroll Compressors Including the Solution of the Temperature Distribution along the Scroll Wraps

Marco C. DINIZ[1], Evandro L. L. PEREIRA[2], Cesar J. DESCHAMPS[1]*

[1]POLO Research Laboratories for Emerging Technologies in Cooling and Thermophysics
Federal University of Santa Catarina
Florianopolis, SC, Brazil
deschamps@polo.ufsc.br

[2]Embraco
Rua Rui Barbosa, 1020
89219-901, Joinville, SC, Brazil
Evandro_L_Lange@embraco.com.br

* Corresponding Author

ABSTRACT

A lumped parameter thermal model has been developed to predict the temperature distribution of scroll compressors with especial attention to gas superheating in the suction process. Thermal resistances between the components were based on global heat transfer coefficients, whereas conduction heat transfer through the scroll wraps was solved via a one dimensional finite volume method. The thermal model was coupled to a thermodynamic model of the compression cycle and then applied to simulate the compressor performance at different conditions of speed and pressure ratio. The model was able to correctly predict the compressor temperature distribution for operating conditions within the range of those adopted for its calibration. The results showed a strong coupling between the compressor thermal profile and the temperatures of the motor and lubricating oil. The model demonstrated that heat conduction through the scroll wraps reduces slightly the discharge temperature.

1. INTRODUCTION

The scroll compressor performs the compression process by using two identical inter-fitting, spiral-shaped scroll elements. These elements are mounted inverted and rotated 180° in relation to each other and, by making contact with each other at sealing points, form multiple compression volumes, hereafter denominated pockets. As the orbiting scroll performs its movement in relation to the stationary scroll, the sealing points migrate inward, pushing the pockets to the center of the scrolls, reducing their volumes and compressing the gas.

In addition to gas leakage, the volumetric and isentropic efficiencies of scroll compressors are affected by heat transfer that takes place inside the pockets during the suction and compression processes. One of the first studies related to heat transfer applied to hermetic scroll compressors was carried out by Wagner *et al*. (1992). The authors experimentally analyzed heat fluxes in different components of the compressor. Other experimental investigations were focused on heat transfer inside the pockets (Jang and Jeong, 1999; Jang and Jeong 2006), and temperature distribution along the scroll wraps (Sunder, 1997; Lin *et al.*, 2005). Numerical models based on lumped formulations have also been developed to estimate the compressor temperature distribution (Lee, 1999; Chen *et al.*, 2002). Other authors (Ooi and Zhu, 2004) have used CFD to predict the temperature of the gas inside the pockets. Recently, Pereira (2012) developed a comprehensive model to characterize the suction, compression and discharge processes of scroll compressors, with correlations especially developed to evaluate leakage and heat transfer in the pockets.

The present paper reports a numerical analysis of the temperature distribution of scroll compressors and its influence on the gas suction temperature. Heat transfer inside the pockets was evaluated via a lumped parameter thermal model and a finite volume model was adopted to predict the temperature profile of the scroll wraps. Both models were coupled to a thermodynamic model for the compression cycle (Pereira, 2012) and simulations were carried out for different operating conditions.

2. EXPERIMENTAL SETUP

The model developed to predict the compressor temperature distribution was calibrated with reference to experimental data. To this extent, an R410A scroll compressor was instrumented with thermocouples in the following positions of interest: compressor inlet, gas suction chamber, compressor outlet, lubricating oil, motor and shell (Figure 1). The compressor was tested at 100% and 80% of its nominal speed. Table 1 presents measurements of the temperature distribution for the evaporating temperature T_e = 7.2°C and different condensing temperatures. Such measurements were used to calibrate the thermal simulation model, as it will be explained shortly.

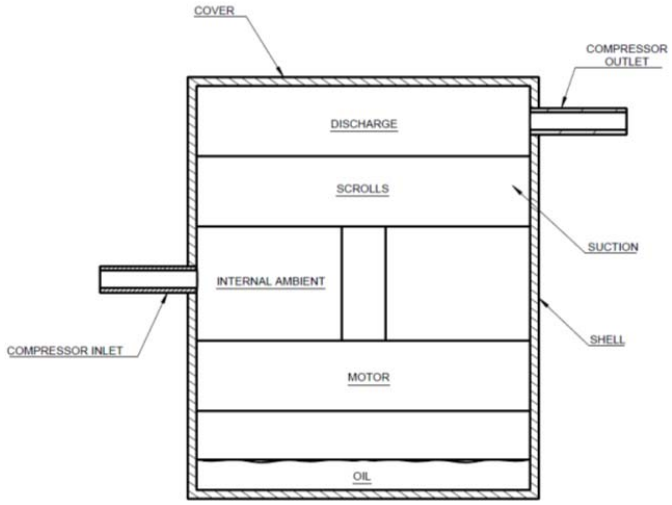

Figure 1: Positions of thermocouple measaments.

Table 1: Compressor temperature distribution for T_e = 7.2°C and different condensing temperatures.

Test	Speed (%)	T_c (°C)	T_{in} (°C)	T_{suc} (°C)	T_{oil} (°C)	T_{mot} (°C)	T_{shl} (°C)
1	80	26.7	21.3	38.5	50.0	46.3	40.1
2	80	37.8	21.4	40.3	46.1	49.2	39.5
3	80	54.4	21.3	44.0	49.3	55.1	40.9
4	100	26.7	20.8	39.5	53.3	48.5	41.7
5	100	37.8	20.8	41.2	53.5	51.4	42.1
6	100	54.4	20.9	44.7	58.0	56.8	43.5

3. NUMERICAL METHOD

3.1 Global Model

Simulations of the compressor temperature distribution were made using a lumped parameter thermal model, in which the enthalpy form of the energy equation was used to describe the energy exchanges in each control volume. For instance, the energy balance for the suction plenum is described as follows:

$$\dot{m}h_{in} + \dot{Q}_{shl->suc} + \dot{Q}_{mot->suc} = \dot{m}h_{suc} \quad (1)$$

On the other hand, the balance inside the compressor pockets is expressed by Equation (2), with the heat dissipated in the discharge region being obtained from Equation (3). Equation (3) is particularly important because it provides the heat released by the discharge chamber into the compressor low pressure region (Equation 4).

$$\dot{m}h_{suc} + \dot{W}_{pv} = \dot{m}h_{dis} + \dot{Q}_{gas->scr} \tag{2}$$

$$\dot{m}h_{dis} = \dot{m}h_{out} + \dot{Q}_{dis->shl} \tag{3}$$

The energy balance applied to the compressor shell provides an equation that is related to the other energy balance equations, guaranteeing conservation of energy in the model.

$$\dot{Q}_{shl->ext} + \dot{Q}_{shl->suc} = \dot{Q}_{oil->shl} + \dot{Q}_{dis->shl} \tag{4}$$

The total amount of heat generated by losses in the electric motor is considered as suction superheating, following Equation (5). Mechanical heat losses due to friction in the bearings, Equation (6), are used to evaluate the oil temperature, which is then included in the energy balance of the compressor shell, Equation (4).

$$\dot{Q}_{mot->suc} = \dot{W}_{ele} - \dot{W}_{shf} \tag{5}$$

$$\dot{Q}_{oil->shl} = \dot{W}_{shf} - \dot{W}_{pv} \tag{6}$$

The indicated power is calculated via a thermodynamic model. For given values of mechanical and electrical efficiencies, shaft power and electrical consumption can be calculated, generating heat sources in the elements representing the motor and the lubricating oil. Figure 2 is a schematic of the thermal resistances that form the model.

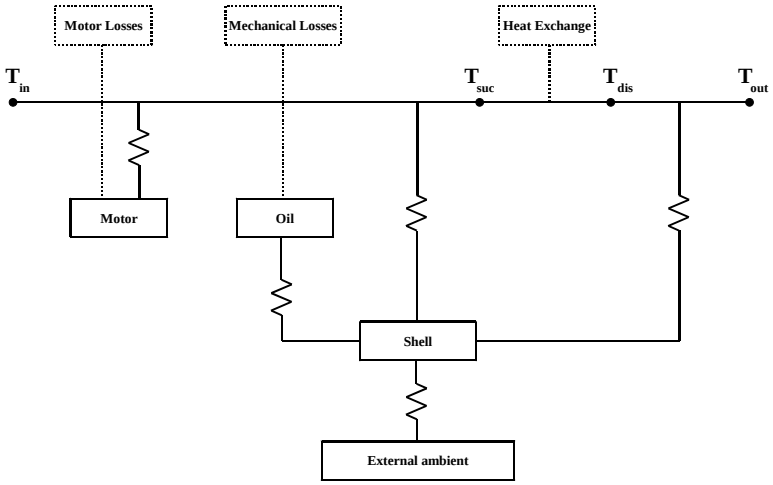

Figure 2: Thermal resistances and elements of the lumped parameter thermal model.

The heat transfer terms in Equations (1)-(6) are represented through global heat transfer coefficients, as shown in Equation (7) for heat transfer between the shell and external ambient.

$$\dot{Q}_{shl->ext} = UA_{shl->ext}(T_{shl} - T_{ext}) \tag{7}$$

The experimental data for temperature in different regions of the compressor allowed the evaluation of all global heat transfer coefficients required in the model. In order to use the model here described for a variety of operating

conditions, calibration curves were adjusted to express the global heat transfer coefficients for a range of condensing temperatures and two compressor speeds.

After being calibrated, the thermal simulation model can be applied to predict the temperature of important compressor components for operating conditions not included in the experiments. The set of equations generated by the energy balances was solved using a Newton-Raphson iterative method. The properties of the gas were obtained by using libraries provided by REFPROP (NIST, 2008).

3.2 Heat Conduction along the scroll wrap

A one-dimensional finite volume model was developed to predict conduction heat transfer and the temperature of the scroll wrap, which is required to evaluate the convective heat transfer inside each compression chamber (pocket).

Figure 3(a) depicts the geometry used to model the conduction heat transfer in the fixed scroll. At a given orbiting angle θ, different regions of the scroll wrap are in contact with suction, compression and discharge gas pockets. The model assumes that fixed and orbiting scrolls have the same temperature profiles. Hence, equations are solved for one wrap only. The scroll wrap was simplified to a stripe, as illustrated in Fig. 3(b). At any time the inward and outward sides of the wrap are in contact with gas at different temperatures. It should be noted that the inward face of any control volume is always in contact with a chamber that contains hotter gas than the outward face of the same control volume. The boundary conditions for the one-dimensional conduction heat transfer in the stripe are set at the discharge point (B) and suction point (A), as shown in Figure 3.

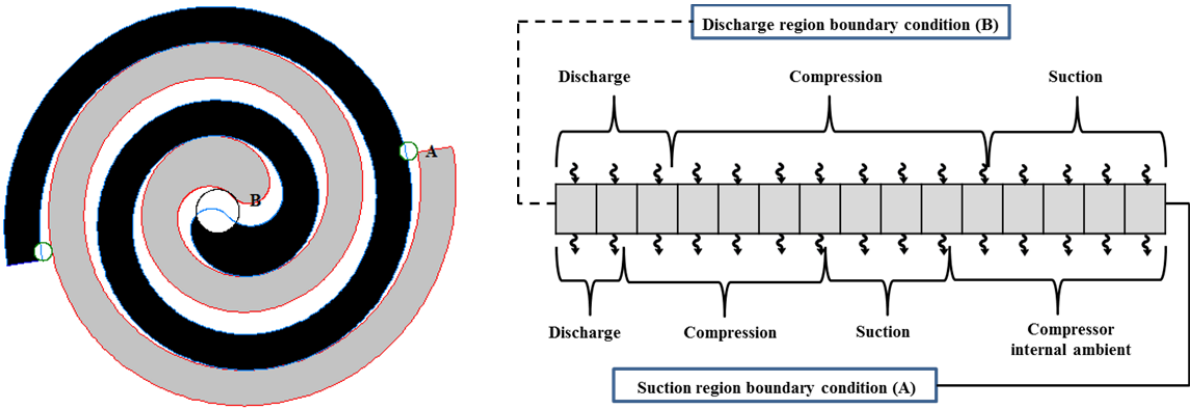

(a) (b)

Figure 3: Scroll wrap: a) actual geometry; b) modeled geometry and discretization volumes.

The differential model for conduction heat transfer in the scroll wraps adopts convective heat transfer coefficients and gas temperatures as boundary conditions, evaluated with the simulation model developed by Pereira (2012). The numerical solution returns the wrap temperature profile needed in the lumped parameter thermal model to evaluate the convective heat transfer between the gas and the scroll wraps throughout the compression cycle. For each control volume in the solid model, the convective heat transfer coefficients on the inward and outward faces are averaged for one complete revolution cycle. The same procedure is applied to obtain averaged gas temperatures facing a certain control volume. A central difference scheme was adopted to interpolate the quantities needed at the control volume faces. The resulting system of linear equations is solved with the TDMA algorithm.

The thermal models described herein were coupled to a thermodynamic model of the compressor, allowing the prediction of the suction gas temperature and, as a consequence, the compressor performance. The discharge temperature is also affected by the scroll wrap temperature and has a major influence on the lumped parameter thermal model. Therefore, the solution procedure follows an iterative approach in which the thermodynamic and thermal models exchange information.

4. RESULTS AND DISCUSSION

4.1 Temperature field results

All numerical results were obtained for the refrigerant R410A and evaporating temperature of 7.2°C. Calibration curves for global heat transfer coefficients were developed considering the compressor operating at 80% and 100% of its nominal speed, and condensing temperatures between 26.7°C and 54.4°C (Table 1). For this reason, the analysis was restricted to this range of operating conditions.

Figure 4 compares experimental and numerical results for temperature in the suction chamber, compressor shell, electric motor and lubricating oil. The results show that the temperatures of the gas in the suction chamber, electric motor and lubricating oil are strongly affected by the condensing temperature. Good agreement between the results is observed for 80% and 100% of the compressor nominal speed. It should be pointed out that the model does not predict the temperature distribution correctly for operating conditions outside the range adopted in its calibration.

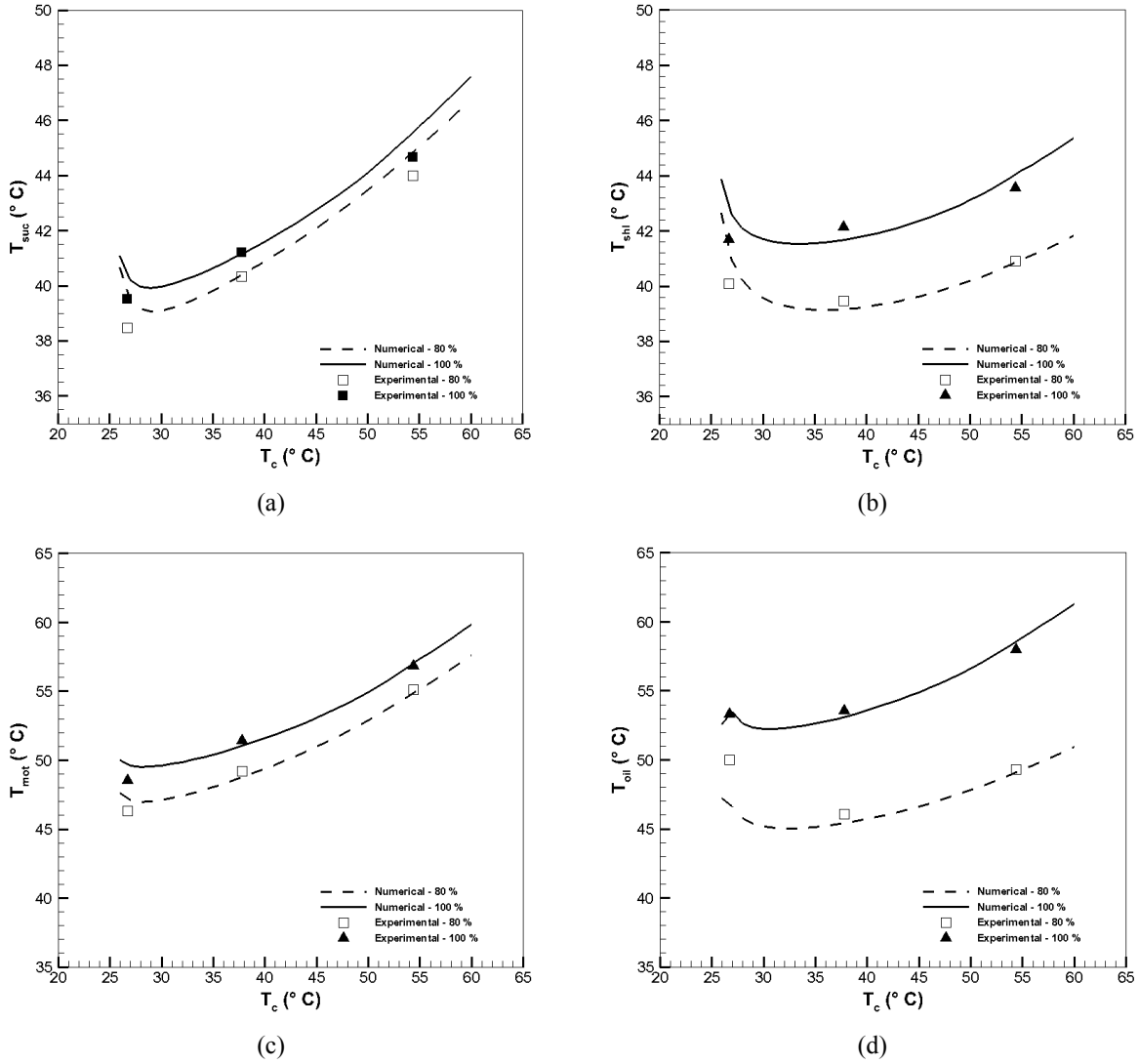

Figure 4: Experimental and numerical results for temperature: (a) suction chamber; (b) compressor shell; (c) electric motor; (d) lubricating oil,

Figure 5 depicts the relation between the suction gas temperature and the temperatures of both the electric motor and the lubricating oil. It can be observed that the temperatures of the motor and of the suction gas vary quite similarly with respect to changes in the compressor operating condition. On the other hand the oil temperature is less sensitive than the suction gas temperature to such variations. An interesting result is that the compressor speed affects more significantly the oil temperature than the motor temperature. This is a consequence of the greater amount of heat due to viscous friction that is released to the oil in the bearings.

Figures 6 and 7 present the influence of mechanical and electrical efficiencies on both the temperature field and the compressor isentropic efficiency, considering T_e = 7.2°C, T_c = 54.4°C and the compressor nominal speed. As can be seen, as the electrical efficiency decreases the motor temperature increases quite sharply (Figure 6b), in the same way as the mechanical efficiency affects the oil temperature (Figure 6a). One can also verify that the mechanical efficiency has a greater impact on the compressor volumetric and isentropic efficiencies (Figure 7).

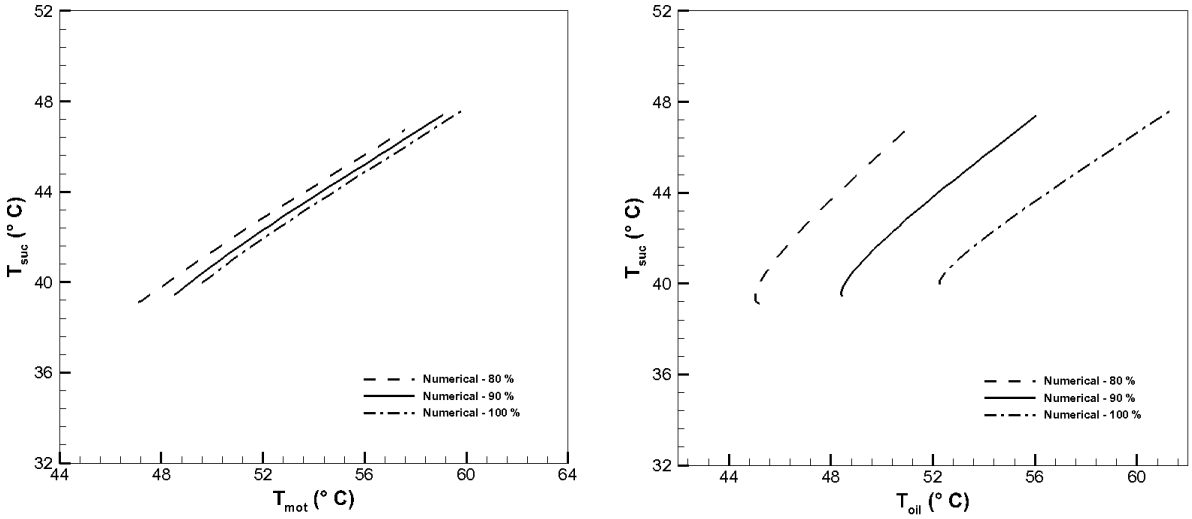

(a) (b)

Figure 5: Relation between the suction temperature and the temperatures of the electric motor (a) and the lubricating oil (b).

The adoption of forced convection on the shell external surface is a well-known alternative to increase heat transfer from the compressor to the external ambient. Figure 8 presents results for the compressor temperature distribution as a function of the global heat transfer coefficient ($UA_{shl->ext}$) characterizing the external convection heat transfer. As expected, there is a direct impact on shell temperature, which appears to be well correlated with the temperatures of the oil and of the suction gas. In fact, the oil temperature is much more affected by the forced convection than the motor temperature. Although the volumetric and isentropic efficiencies increase with global heat transfer coefficient $UA_{shl->ext}$, such an increase assumes an asymptotic behavior after the value of $UA_{shl->ext}$ is tripled.

4.2 Heat Conduction in the Scroll Wraps

The temperature of the scroll wraps is required as boundary condition in the evaluation of convective heat transfer inside the compressor pockets. Numerical predictions with the finite volume method are prone to truncation errors and therefore tests of grid refinement were carried out, by prescribing the suction and discharge temperatures at the scroll extremities (points A and B in Figure 3). Results for temperature distribution in Figure 9 show that the use of 1000 volumes in the discretization is sufficient to guarantee negligible truncation error.

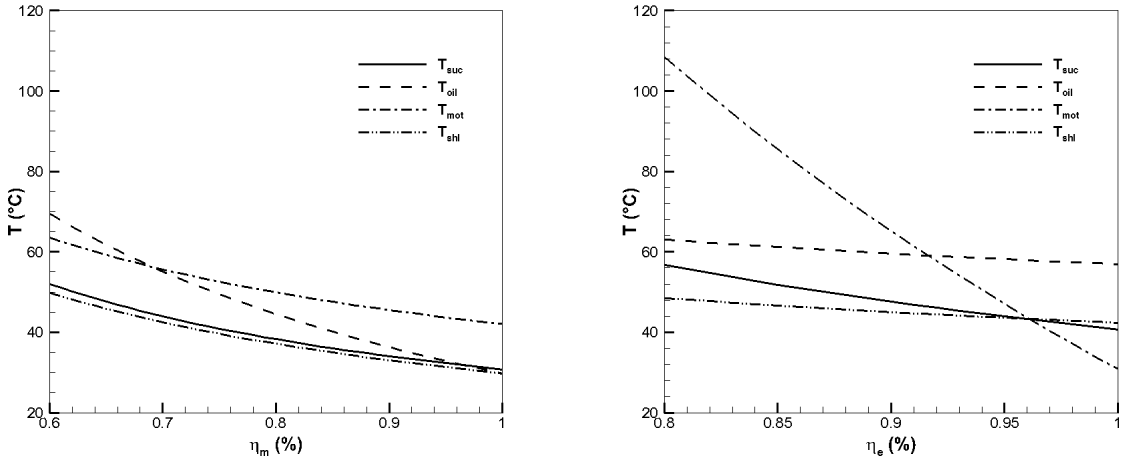

(a) (b)

Figure 6: Influence of mechanical efficiency (a) electrical efficiency (b) on the temperature distribution.

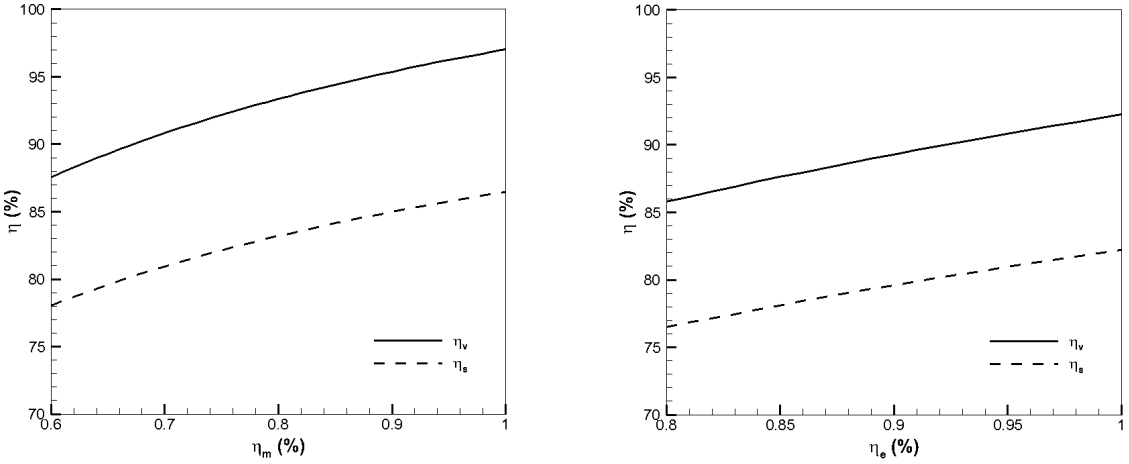

(a) (b)

Figure 7: Influence of mechanical efficiency (a) electrical efficiency (b) on the compressor efficiencies

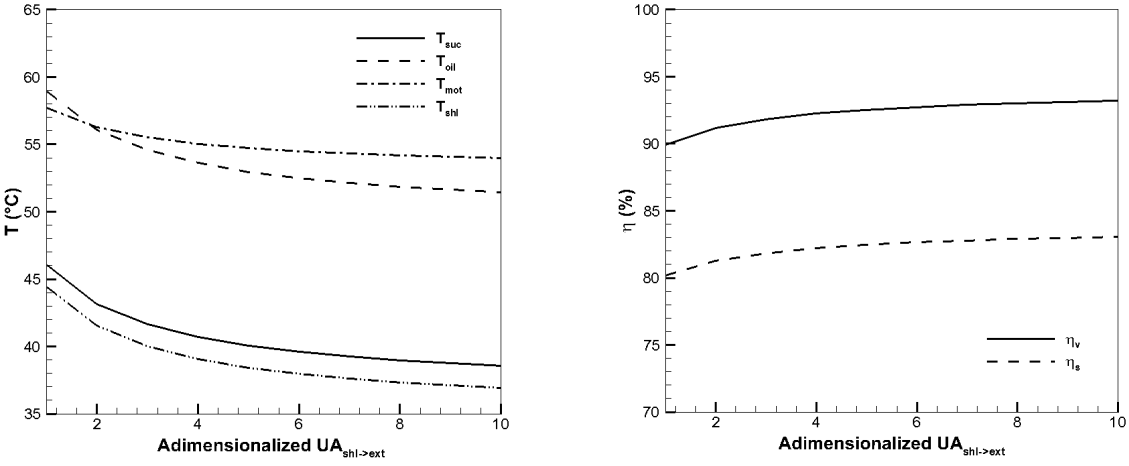

(a) (b)

Figure 8: Influence of external forced convection on (a) temperature distribution and (b) compressor efficiencies.

Figure 10 presents predictions of temperature distribution along the scroll obtained with different boundary conditions at point B of the scroll wrap, shown in Figure 3: i) adiabatic condition; ii) convective heat transfer h = 1000 W/(m^2 K); iii) prescribed temperature $T_B = T_{dis}$. Different types of boundary condition were also tested at the other extremity (point A), but very little variation was verified in the scroll wrap temperature profile. Therefore, results presented in Figure 10 are for a fixed boundary condition at point A (h = 100 W/(m^2 K). The commonly adopted linear temperature variation adopted in most thermal simulations of scroll compressors is also shown in Figure 10 for reference.

The results show that the scroll wrap temperature has a small increase in the outer region because the gas enters the pockets with lower temperature in the suction process. Hence, heat is transferred from the wrap surface to the gas in this region. Eventually the gas temperature becomes higher than the scroll temperature and heat transfer occurs in the opposite direction, with the scroll wrap temperature increasing rapidly as a result of the compression process. One can notice from Figure 10 that the boundary condition at point B affects considerably the temperature of the scroll wrap close to the discharge chamber.

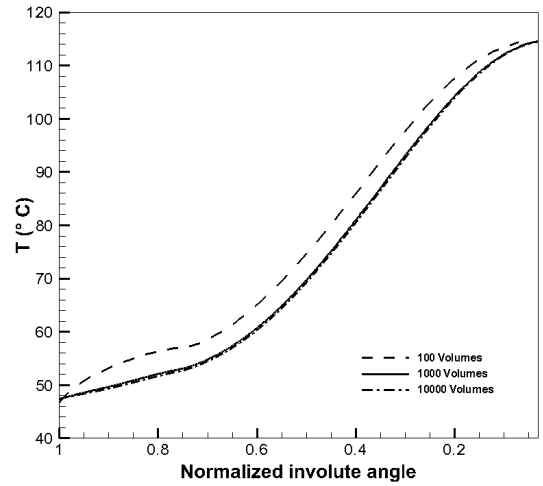

Figure 9: Grid refinement tests.

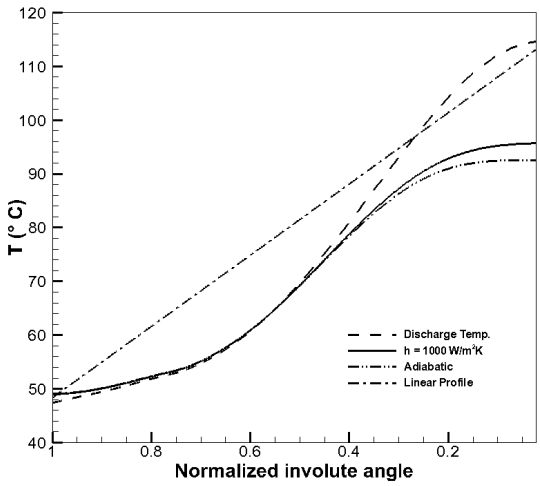

Figure 10: Temperature distribution in the scroll wrap.

Figure 11 presents the temperature distribution in the scroll wrap when different percentages of the thermal energy in the discharge chamber are assumed to be transferred to the scroll wrap. Since the boundary condition is an important parameter of the numerical simulation, two different conditions were adopted: i) prescribed temperatures at points A ($T = T_{suc}$) and B ($T = T_{dis}$); (b) prescribed convective heat transfer coefficients at points A (h = 100 W/m^2/K) and B (h = 1000 W/m^2/K). It can be observed that heat released from the discharge chamber affects the scroll wrap temperature, which justifies further study of this aspect in the future. This phenomenon can explain in part the distinction between the temperature distributions of the fixed and orbiting scrolls, since the heat flux on their base plates is quite different. In fact, the temperature profile of the fixed scroll is well correlated with the discharge gas temperature, whereas the temperature of the orbiting scroll is better related with viscous friction heat dissipation in the thrust bearing.

Finally, Figure 12 presents results for the gas discharge temperature as a function of condensing temperatures, predicted by the thermal model with and without solving the one-dimensional heat conduction along the scroll (SHC) via the finite volume method. A linear temperature profile was assumed when heat conduction was not solved. It is clear from Figure 12 that a lower discharge temperature is predicted when heat conduction is included in the numerical analysis.

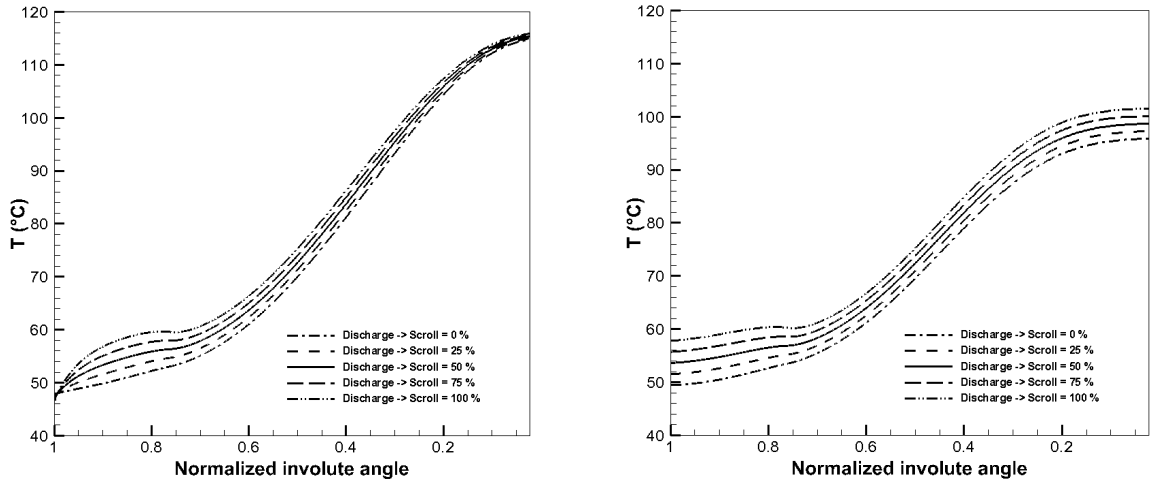

Figure 11: Influence of heat released from the discharge chamber on the scroll temperature distribution: (a) Temperatures prescribed at points A and B; (b) Convective heat transfer prescribed at points A and B.

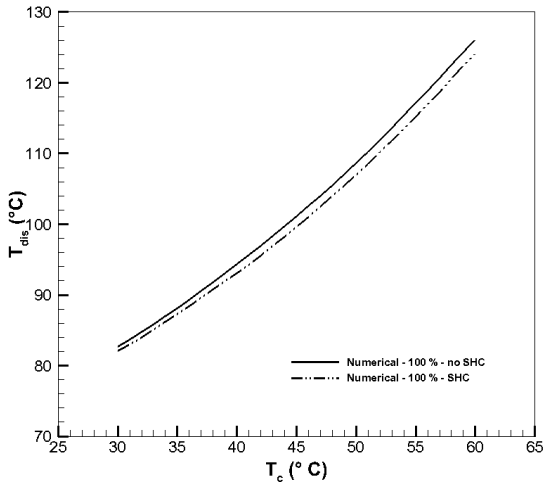

Figure 12: Discharge temperature variation with and without heat conduction in the scroll (SHC).

5. CONCLUSIONS

This paper presented a numerical model developed to predict the temperature distribution of a scroll compressor, with heat conduction along the scroll wraps being solved via a finite volume model. Results show that the suction gas temperature is better correlated with the oil temperature than with the electric motor temperature. As the compressor speed is increased mechanical losses play a major role in the compressor temperature distribution, reducing its volumetric and isentropic efficiencies. The model was based on global heat transfer coefficients and its application was showed to be limited to operating conditions within the range of those adopted for its calibration. Heat transfer from the gas inside the discharge chamber to the scroll base plate was seen to have a significant influence on the scroll temperature distribution.

NOMENCLATURE

h_{in}	Specific enthalpy at inlet	(J/kg)	T_{ext}	External ambient temperature	(°C)
h_{dis}	Specific enthalpy at discharge	(J/kg)	T_{in}	Compressor inlet temperature	(°C)
h_{out}	Specific enthalpy at outlet	(J/kg)	T_{mot}	Motor temperature	(°C)
h_{suc}	Specific enthalpy at suction	(J/kg)	T_{oil}	Oil temperature	(°C)
$\dot{m}$	Mass flow rate	(kg/s)	T_{shl}	Shell temperature	(°C)
$\dot{Q}_{dis->shl}$	Heat transfer from discharge chamber to shell	(W)	T_{suc}	Suction temperature	(°C)
$\dot{Q}_{gas->scr}$	Heat transfer from gas to scroll	(W)	$UA_{shl->ext}$	Global heat transfer coefficient	(W/K)
$\dot{Q}_{mot->suc}$	Heat transfer from motor to suction gas	(W)	$\dot{W}_{ele}$	Electrical consumption	(W)
$\dot{Q}_{oil->shl}$	Heat transfer from oil to shell	(W)	$\dot{W}_{pv}$	Indicated Power	(W)
$\dot{Q}_{shl->ext}$	Heat transfer from shell to external ambient	(W)	$\dot{W}_{shf}$	Shaft Power	(W)
$\dot{Q}_{shl->suc}$	Heat transfer from shell to suction gas	(W)	η_e	Electrical efficiency	( )
T_c	Saturated condensing temperature	(°C)	η_s	Isentropic efficiency	( )
T_{dis}	Discharge temperature	(°C)	η_m	Mechanical efficiency	( )
T_e	Saturated evaporating temperature	(°C)	η_v	Volumetric efficiency	( )

REFERENCES

Chen, Y., Halm, N.P., Groll, E.A., Braun, J.E., 2002, "Mathematical modeling of scroll compressors – part II: overall scroll compressor modeling", *Int. J. Refrig*., vol. 25, p. 751-764.

Jang, K., Jeong, S., 1999, "Temperature and heat flux measurement inside variable-speed scroll compressor", Proc. Int. Congress of Refrigeration, pp. 97-106.

Jang, K., Jeong, S., 2006, "Experimental investigation on convective heat transfer mechanism in a scroll compressor", *Int. J. Refrig*., vol. 29, p. 744-753.

Lin, C., Chang, Y., Liang, K., Hung, C., 2005, "Temperature and thermal deformation analysis on scrolls of a scroll compressor", *Applied Thermal Engineering*., vol. 25, p. 1724-1739.

NIST, National Institute of Standards and Technology, 2008, "Refprop - Reference fluid thermodynamic and transport properties", v. 8, USA.

Pereira, E.L.L., 2012, "Modeling and analysis of the thermodynamic performance of scroll compressors", Ph.D. Thesis, Federal University of Santa Catarina, (in Portuguese).

Sunder, S., 1997, "Thermodynamic and heat transfer modeling of a scroll compressor", Ph.D. Thesis, Massachusetts Institute of Technology.

Wagner, T.C., Marchese, A.J., McFarlin, D.J., 1992, "Characterization of thermal processes in scroll compressors", Proc. Int. Compressor Engineering Conference at Purdue University, pp. 97-106.

ACKNOWLEDGEMENTS

The present study was developed as part of a technical-scientific cooperation program between the Federal University of Santa Catarina and EMBRACO. The authors also thank the support of CNPq (National Council of Research) through grant 573581/2008-8 (National Institute of Science and Technology in Refrigeration and Thermo physics) and CAPES (Coordination for the Improvement of High Level Personnel).